Curvature effects in rapid alloy solidification

Massimo Conti
Dipartimento di Matematica e Fisica, Universitá di Camerino, and Istituto Nazionale di Fisica della Materia, Via Madonna delle Carceri, I-62032, Camerino, Italy

(Received 22 February 2000; revised manuscript received 19 July 2000; published 27 March 2001)

The growth of a cylindrical or spherical crystal into its undercooled melt is a process whose description is complicated by the lack of a stationary regime. A simple approach to the problem, justified for low growth rates and widely used in the past for both pure substances and alloy solidification, is based on a quasistatic approximation which assumes an instantaneous adaptation of the diffusional field to the interface configuration. For alloy solidification, assuming isothermal conditions and local interface equilibrium, this simplified model predicts a diffusion controlled growth, with the radius of the crystal increasing asymptotically as $\propto t^{1/2}$. However, as pointed out by recent investigations, thermal diffusion and nonequilibrium effects enter as essential ingredients in rapid alloy solidification. In the present paper we use the phase-field model to simulate the cylindrical and spherical growth of a solid germ into a supersaturated alloy melt. The problem is treated in its full time-dependent characteristics, accounting for nonequilibrium effects as well as for the rejection of both heat and solute away from the advancing front. We observe a complex behavior and a rich variety of dynamic regimes: in different regions of parameter space the growth rate is limited by diffusion (either thermal or chemical) or is kinetic controlled. Traversing the boundaries which limit these regions, the process undergoes sharp transitions which leave a trace in the solidified alloy. For realistic values of the Lewis number, thermal effects drive the process into a a diffusive regime, in which the rate limiting mechanism is the rejection of solute.

DOI: 10.1103/PhysRevE.63.041507 PACS number(s): 64.70.Dv, 81.15.Lm, 81.30.Bx, 68.35.Md

I. INTRODUCTION

In rapid solidification of binary alloys the growth rate is controlled by the diffusive transport of both heat and solute away from the advancing front. A classical (sharp interface) description of the process couples the diffusion equations in the bulk phases with interfacial boundary conditions. The latter consist of two different constraints: (a) energy and solute conservation across the moving front, and (b) constitutive laws which relate the concentration c and temperature T at the interface to the front velocity v. As the relaxation of the thermal field is much faster than the rearrangement of chemical species, the process is often treated as isothermal. In this limit Langer [1] pointed out that, assuming local interfacial equilibrium, and considering the chemical potential rather than the concentration field, the model for alloy solidification is reduced to the same set of governing equations which describe the solidification of a pure substance. However, at large growth rates nonequilibrium effects become dominant: the solid-liquid front requires a large undercooling to advance, and the partition coefficient k (i.e., the ratio c_s/c_l of solute concentration in the growing solid to that in the liquid at the interface) increases from the equilibrium value k_e toward unity, reflecting the trapping of solute into the solid phase. These phenomena were addressed in several studies by Aziz and co-workers [2–4] through the continuous growth model. Starting from a mesoscopic analysis of the diffusive processes within the interfacial boundary layer, they were able to derive a dynamic phase diagram, showing that the interface temperature is a nonmonotonic function of the growth rate.

A diffuse interface approach to study alloy solidification is based on the phase-field model (PFM). A phase field $\phi(x,t)$ characterizes the phase of the system at each point; a free-energy (or entropy) functional, depending on ϕ, T, and c, as well as on their gradients, is then extremized in respect to these variables, to derive the dynamic equations for the process. Several theoretical and numerical studies [5–12] pointed out that the PFM describes, in a natural fashion, nonequilibrium effects like solute trapping and the kinetic undercooling of the solid-liquid interface.

Employing these models, alloy solidification has been studied in different regimes, generally neglecting the diffusion of the thermal field. Much attention has been devoted to the dynamics and instabilities of a planar interface growing either in an adverse temperature gradient or into a supersaturated melt (see Refs. [13–15] for a review). In the latter case it is always possible, choosing proper conditions at infinity, to find a stationary regime in which the solid grows at a constant velocity.

A different picture arises when cylindrical (or spherical) growth is considered, as in this case the process cannot be stationary. The evolution of the interface dynamics, in the isothermal limit, can be addressed within the quasistatic approximation: the time-dependent diffusion equation is replaced by the Laplace's equation which satisfies all the boundary conditions except the solute conservation at the moving front; the latter is then utilized to determine the interface velocity. Assuming local interfacial equilibrium, the solution of this simplified model shows that the growth is limited by solute diffusion [16]; as the radius R of the crystal increases (and curvature effects become negligible), the well known $R \propto t^{1/2}$ power law is asymptotically approached. The stability of the spherical solution against small deformations of the solid germ was treated by Mullins and Sekerka; in their seminal paper [17] they found that the spherical nucleus

begins to deform when its radius exceeds a critical value which is just seven times the nucleation radius.

The quasistatic approximation, which assumes an instantaneous adaptation of the diffusive field to the actual interface configuration, is justified only at low growth rates. At large values of the dimensionless supersaturation $\Delta=(c_l^*-c_\infty)/(c_l^*-c_s^*)$ (where c_∞ represents the initial solute concentration of the melt and c_l^* and c_s^* are the equilibrium solute concentrations in the liquid and solid phases, respectively), the problem should be treated in its full time-dependent characteristics and taking into account nonequilibrium effects. Moreover recent investigations pointed out that thermal diffusion enters as an essential ingredient into the evolution of the phase-change process [18–20].

In the present paper the cylindrical or spherical growth of a solid germ is simulated with the phase-field model. The study is conducted in one dimension, so that the morphological instabilities of the solid-liquid interface are beyond the scope of our analysis. We focus on the dynamics of the process at large supersaturation accounting, for both thermal and solute diffusion. Depending on the value of the Lewis number (i.e., the ratio of the chemical to the thermal diffusivity), the growth process reveals an unsuspected variety of dynamic regimes. At Le$=0$ (the isothermal limit), during an initial transient, the growth is limited by solute diffusion. The interface velocity decreases with time, and the solute segregation approaches the equilibrium pattern. Then, at a certain value R^* of the crystal radius, the effective supersaturation at infinity becomes large enough to drive the process into a different regime in which the limiting mechanism is the finite rate of the atomic attachment. The growth velocity increases abruptly by several orders of magnitude, and asymptotically approaches the value found for planar growth; this stage is characterized by a strong trapping of solute in the solid phase.

At small but finite values of the Lewis number the growth rate first decays, as limited by chemical diffusion. The release of solute ceases to be an obstacle to the interface advancement when the crystal radius reaches a characteristic value R^*; here we observe the already mentioned abrupt increase of the interface velocity. But now the finite value of the thermal diffusivity prevents the evolution of the process into the kinetic controlled regime, and the growth is limited by thermal diffusion. In this high velocity stage the interface temperature increases with time, and solute is strongly trapped into the solid phase. Then, when the interface temperature reaches a value near the T_0 line (where the Helmoltz free energies of the liquid and solid are equal), a sharp transition again turns the process into a low velocity regime. This transition was already identified by the author [20] in a previous study on planar solidification. The interface temperature is now decreasing with time, and the solute segregation at the interface approaches the equilibrium pattern. It should be noted that this complex behavior occurs in a region of the parameters space which is not accessible to metallic alloys.

With Le values characteristic of metallic alloys, thermal effects drive the solidification process into a diffusive regime governed by the rejection of solute at the interface, and the front velocity decays with time, asymptotically approaching the $v\propto t^{-1/2}$ power law.

The paper is organized as follows: in Sec. II the governing equations of the model will be derived, through the extremization of an entropy functional. In Sec. III the numerical method will be explained, and in Sec. IV the results of the numerical simulations will be discussed. The conclusions will follow in Sec. V.

II. GOVERNING EQUATIONS

The model follows the formulation given by Warren and Boettinger [21] and also incorporates many of the ideas developed by Caginalp and Xie [5], Caginalp and Jones [6], and Wheeler *et al.* [7,8]. Full details of the derivation are presented elsewhere [22], and will not repeated here.

The entropy of an ideal solution of components A (solvent) and B (solute) is written as

$$\mathcal{S}=\int\left[s(e,\phi,c)-\frac{\epsilon^2}{2}|\nabla\phi|^2\right]dv, \tag{1}$$

where s and e are the local densities of the thermodynamic entropy and the internal energy, respectively, and ϕ is the order parameter which assumes the values $\phi=0$ in the solid and $\phi=1$ in the liquid. The last term in the integrand is a gradient correction which accounts for the thermodynamic cost of the interface. To ensure a positive local entropy production, functional (1) is extremized, generating the dynamic equations for the process. It is convenient to formulate the problem in nondimensional form, scaling lengths to some reference length ξ and time to ξ^2/D_l, D_l being the solute diffusivity in the liquid phase. Then the field equations become:

$$\frac{\partial\phi}{\partial t}=[(1-c)m^A+cm^B][\nabla^2\phi+(1-c)Q^A(T,\phi)+cQ^B(T,\phi)], \tag{2}$$

$$\frac{\partial c}{\partial t}=-\nabla\cdot\{c(1-c)\lambda(\phi)[H^A(\phi,T)-H^B(\phi,T)]\nabla\phi+c(1-c)\lambda(\phi)\Gamma(\phi,T)\nabla T-\lambda(\phi)\nabla c\}, \tag{3}$$

$$\frac{\partial T}{\partial t}=\frac{1}{\mathrm{Le}}\nabla^2T-\frac{1}{\chi}[(1-c)L^A+cL^B]\frac{dp(\phi)}{d\phi}\frac{\partial\phi}{\partial t}-\frac{1}{\chi}p(\phi)\times(L^B-L^A)\frac{\partial c}{\partial t}, \tag{4}$$

where Le is the Lewis number, defined as the ratio Le $=D_c/D_T$ of the chemical to the thermal diffusivity; $L^{A,B}$ represents the latent heat per unit volume of the component A or B; and χ is the specific heat, for which we assume equal values for both components in both phases. The function $p(\phi)$, defined as $p(\phi)=\phi^3(10-15\phi+6\phi^2)$, enforces the condition that the bulk solid and liquid are described by $\phi=0$ and 1, respectively, for every value of temperature [23].

We also define:

TABLE I. Material parameters for the Ni-Cu Alloy.

Parameter	Nickel	Copper
T_m(K)	1728	1358
L(J/cm^3)	2350	1728
v_m(cm^3/mole)[a]	7.0	7.8
σ(J/cm^2)	3.7×10^{-5}	2.8×10^{-5}
β(cm/K s)[b]	128.64	153.60
D_l(cm^2/s)	10^{-5}	10^{-5}

[a]An average value of 7.4 will be taken.
[b]From the estimation of Willnecker *et al.* [24].

$$H^{A,B}(\phi,T)=W^{A,B}\frac{dg(\phi)}{d\phi}-L^{A,B}\frac{v_m}{\bar{R}}\frac{dp(\phi)}{d\phi}\frac{T-T^{A,B}}{TT^{A,B}}, \tag{5}$$

$$Q^{A,B}(\phi,T)=-\frac{\xi^2}{(h^{A,B})^2}\frac{dg(\phi)}{d\phi}+\frac{1}{6\sqrt{2}}\frac{\xi^2L^{A,B}}{\sigma^{A,B}h^{A,B}}\frac{T-T^{A,B}}{T_\infty}\frac{dp(\phi)}{d\phi}, \tag{6}$$

$$\Gamma(\phi,T)=-\frac{v_m}{\bar{R}}\frac{p(\phi)}{T^2}(L^A-L^B), \tag{7}$$

where $g(\phi)=\phi^2(1-\phi)^2/4$ is a symmetric double well potential with equal minima at $\phi=0$ and 1; $T^{A,B}$ is the melting temperature of pure A or B; $\bar{R}$ is the gas constant; and v_m is the molar volume. In Eq. (6), $\sigma^{A,B}$ and $h^{A,B}$ indicate the surface tension and the interface thickness of the components A and B, respectively; T_∞ is the initial melt temperature. The solute diffusivity D_c is scaled as

$$\frac{D_c}{D_l}=\lambda(\phi)=\frac{D_s}{D_l}+p(\phi)\left(1-\frac{D_s}{D_l}\right), \tag{8}$$

allowing for different values D_s and D_l in the solid and liquid phases.

The model parameters $m^{A,B}$ and $W^{A,B}$ depend on the physical properties of the alloy components through [21]

$$m^{A,B}=\frac{\beta^{A,B}\sigma^{A,B}T^{A,B}}{D_lL^{A,B}}, \quad W^{A,B}=\frac{12}{\sqrt{2}}\frac{v_m}{\bar{R}}\frac{\sigma^{A,B}}{T^{A,B}h^{A,B}}, \tag{9}$$

where $\beta^{A,B}$ is the kinetic undercooling coefficient of pure A or B, that relates the interface temperature T_I to the interface velocity v through $v=\beta^{A,B}(T^{A,B}-T_I)$.

To conduct the numerical simulations we referred to the phase diagram of an ideal solution of nickel (solvent) and copper (solute), using the data summarized in Table I; the solute diffusivity in the solid phase was estimated as $D_s=10^{-6}\times D_l$. The length scale was fixed at $\xi=2.1\times10^{-4}$ cm; the kinetic undercooling coefficients were fixed to $\beta^A=128.64$ cm s^{-1} K^{-1} and $\beta^B=153.60$ cm s^{-1} K^{-1}, not far from the actual best estimates [24], and a realistic value for the interface thickness was selected as 1.68×10^{-7} cm. Using the above values it was found that $W^A=0.963$, $W^B=0.960$, and $m^A=m^B=350$.

III. NUMERICAL METHOD

Equations (2)–(4) have been expressed in cylindrical or spherical coordinates, and solved for the sole spatial variable r, the radial distance. Initially in the supersaturated melt, at uniform temperature and concentration T_∞ and c_∞, a solid germ is nucleated in the region $0\leqslant r\leqslant R_0$, with a composition equal to c_∞. The size of the initial radius is the minimum required to avoid remelting and to ensure the successive growth. To discretize the equations, second order in space and first order in time finite-difference approximations were utilized. Then an explicit scheme was employed to advance the phase field and concentration equations forward in time; the temperature equation was more conveniently integrated with a fully implicit method. The choice of the computational grid posed some delicate problems. The physical process involves intrinsic and quite different length scales. The width of the phase-field and concentration transition layer, across the interface, is of the order of 10^{-3} (nondimensional units); the solute diffusion length, in our simulations, was in the range 10^{-2}–10^0 while the thermal diffusion length reached values as high as 10^4. The necessity to avoid finite-size effects and, at the same time, to resolve the phase and concentration fields accurately, suggested dividing the computational domain into two parts: an inner region, of interest for the phase and concentration dynamics, and an outer region, where only the temperature equation was integrated. In the inner region $0\leqslant r\leqslant r_i$ the grid spacing was selected as $\Delta r_i=4\times10^{-4}$, that is half of the nominal interface thickess. This value was a standard choice in previous studies [9,10,25], where it was proven to ensure accurate solutions of the phase ad concentration equations. In the outer region $r_i\leqslant r\leqslant r_o$, we used a nonuniform grid, stretching the mesh spacing with the law $\Delta r_o=\Delta r_i+\Delta r_\infty[1-\exp((r-r_i)/r_L)]$. The values of Δr_∞ and r_L were chosen, for each simulation, to ensure accuracy as well as computational economy; in any case the temperature field was never resolved with less than 4×10^4 grid points, and the temperature differences between adjacent grid points never exceeded 10^{-3} K.

For the same reason of computational economy, even along the time axis we used different grids. The concentration equation (3) requires, for numerical stability, a time step Δt_c which scales as $(\Delta r)^2/D_l$, where $D_l=1$. On the other hand, the phase-field equation (2) is a diffusion-reaction equation with diffusivity $D_\phi=m^{A,B}=350$; in this case the time step for stability Δt_ϕ is expected to scale as $(\Delta r)^2/D_\phi$. No stability problems arise for the temperature equation, which is integrated with an implicit method with a time step $\Delta t_T=\Delta t_c$. Due to the large value of D_ϕ, we used a value for Δt_ϕ much smaller than $\Delta t_T=\Delta t_c$. In practice we iterated the phase-field equation 320 times within a single time step (equal to 5×10^{-8}) of the temperature and concentration equations.

The convergence of the numerical scheme was checked accurately in different cases with respect to the refinement of

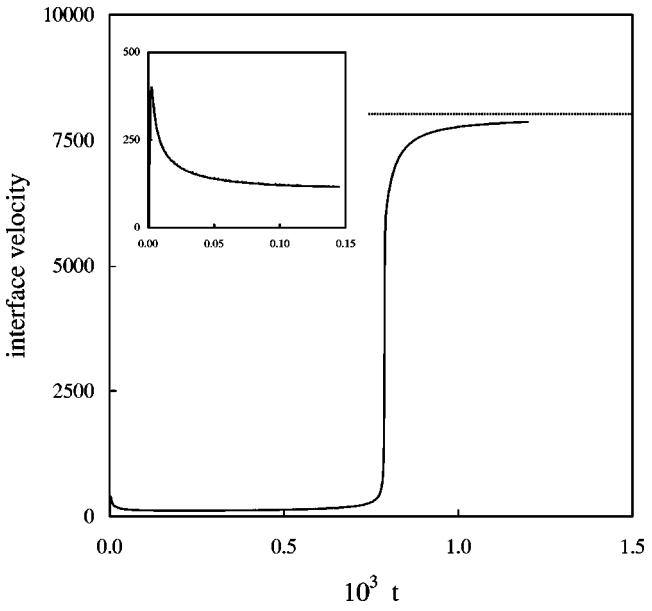

FIG. 1. Cylindrical growth: the interface velocity vs time for the isothermal case. We show (dotted line) the steady interface velocity for a planar interface growing with the same conditions at infinity. The inset represents an enlarged view of the early stage of the process.

the computational grid in both the outer and inner regions; moreover, we checked that using a different time step for the phase-field equation had no influence on the numerical results.

IV. NUMERICAL RESULTS

We fixed $T_\infty = 1700$ K, corresponding to equilibrium concentrations, on the solidus and liquidus lines, respectively: $c_s^* = 0.071611$ and $c_l^* = 0.089945$; the concentration of the melt was set to $c_\infty = c_s^*$ on the solidus line. We first analyze the numerical results for the two-dimensional version of the model. The most relevant features which characterize the evolution of the process are shared by cylindrical and spherical growth, so that the extension of our discussion to the three-dimensional case will be straightforward.

A. Cylindrical growth

The initial radius of the germ was chosen as $R_0 = 0.04$. Here and in the following, except for temperature, physical quantities will be expressed in nondimensional units. The initial conditions correspond to a dimensionless supersaturation $\Delta = 1$ for a planar interface but, due to the Gibbs-Thomson effect, the effective supersaturation is $\Delta < 1$ for the solid germ (and, in general, for a convex interface).

It is interesting to focus on the process dynamics at fixed temperature (which is the limit of the model for $\mathrm{Le} \to 0$). Figure 1 shows the interface velocity versus time; the dotted line indicates the value $v = 7973$, which is the steady velocity for a *planar front* growing with the same conditions at infinity. We observe that in a first stage (see the expanded portion of the graph) the growth rate increases, reaches a maximum and then decreases. This is the expected behavior of a supercritical nucleus, as the driving force for solidification (the supersaturation) is contrasted by the release of solute at the interface, which must be rejected via chemical diffusion. Subsequently the solidification front is accelerated until we observe an abrupt transition: the growth rate increases by about two orders of magnitude and asymptotically approaches the value found for a planar interface. The origin of this transition can be explained by resorting to a picture of the process given by the continuous growth model. We recall that the latter describes the interface kinetics through a dynamic phase diagram expressed, for a dilute alloy, by the equations

$$T_I(v) = T^A + \frac{m_l c_l}{1-k_e}[1-k+(k+(1-k)\gamma)\ln(k/k_e)] - \frac{v}{\beta^A}, \tag{10}$$

$$k(v) = \frac{k_e + v/v_d}{1+v/v_d}, \tag{11}$$

where k_e is the equilibrium partition coefficient for a stationary interface ($k_e = 0.797$ in our case), and v_d is a diffusional velocity for the solute redistribution across the moving front. The slope of the equilibrium liquidus line is indicated as m_l, and the parameter γ describes the extent of the dissipation of free energy due to solute drag across the interface. A previous investigation [10] identified best values of $v_d = 290$ and $\gamma = 0.65$. To adapt these equations to a curved front of radius R, the actual melting temperature of the solvent must be replaced by [26] $T^A[1-(1/R)(\sigma^A/L^A)]$, the equilibrium partition coefficient by $k' = k_e[1-(1/R)(v_m\sigma^A)/(\bar{R}T^A)]$, and the liquidus slope by $m_l' = m_l(1-k')/(1-k_e)$. With these changes, having prescribed the interface temperature, Eqs. (10) and (11) can be solved for the v,R pair consistently with a kinetic controlled growth. In Fig. 2 we show the $v(R)$ dependence, as extracted from Eqs. (10) and (11) (solid dots), compared with the results of the numerical simulation (solid line). The two curves intersect at $R^* = 0.127$: this means that, due to the interface curvature (and the consequent decrease of the effective supersaturation) the kinetic controlled regime is allowed only for $R > R^*$. Indeed, as we observe in the graph, this is just the onset of the transition. In the later evolution of the process the two curves collapse, indicating that the kinetic regime has been reached. The inset of Fig. 2 shows c_s and c_l versus time, i.e., the solute concentration on the solid and liquid sides of the interface. The segregation pattern reflects the time dependence of the solidification rate: at low velocities the solute redistribution is effective and the concentration gap is high; subsequent to the abrupt increase of the growth rate, we observe that solute is trapped into the solid and the partition coefficient approaches unity.

A different picture emerges when the dynamics of the thermal field is taken into account, assuming a high but finite thermal diffusivity. We set $D_T = 15.5 \times 10^7$, that is larger than the actual values characteristic of metallic alloys by a factor of 10^4; this means $\mathrm{Le} = 6.45 \times 10^{-9}$. Figure 3 shows the interface velocity (solid line) and temperature (solid dots)

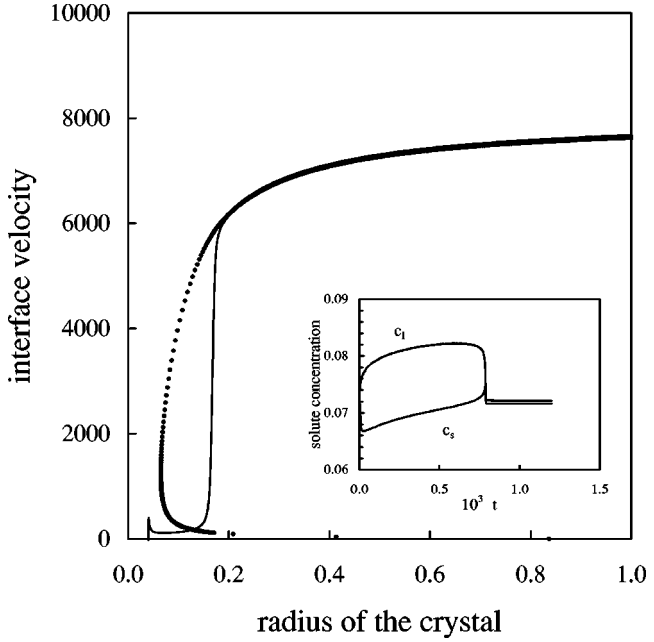

FIG. 2. Cylindrical growth: the interface velocity vs the crystal radius for the isothermal case. Solid line: the results of the present simulation. Solid dots: the solution of Eqs. (10) and (11). The inset represents the solute concentration at the interface vs time.

versus time. The growth rate first decays, as limited by chemical diffusion; in this stage the interface temperature shows a slow increase. When the release of solute ceases to be an obstacle to the interface advancement, we observe the above mentioned abrupt acceleration of the solidification front. But now, due to the finite value of the thermal diffusivity the interface warms up and the growth rate decreases as limited by thermal diffusion. In this high velocity stage

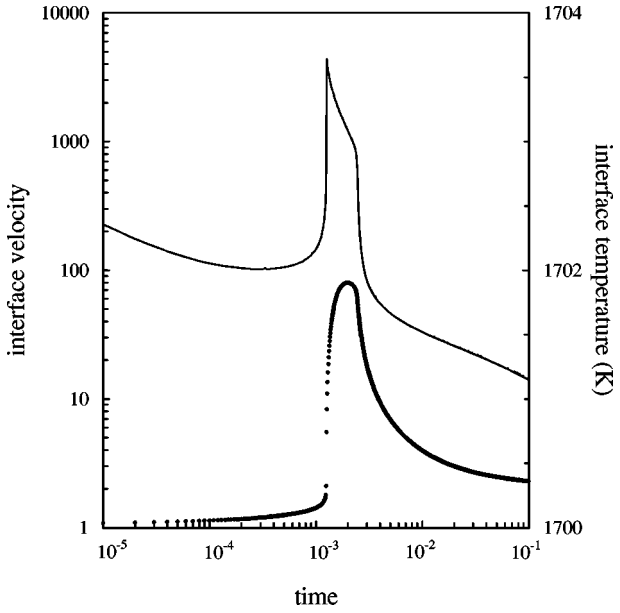

FIG. 3. Cylindrical growth: the interface velocity (solid line) and temperature (solid dots) vs time. The Lewis number is Le $=6.45\times10^{-9}$.

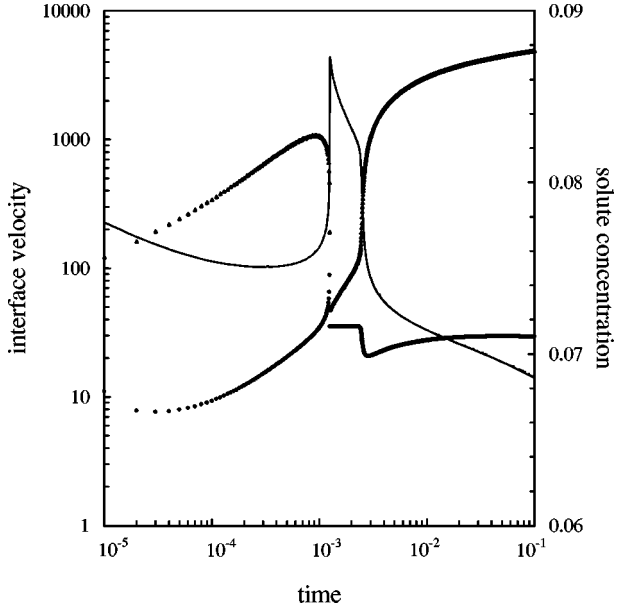

FIG. 4. Cylindrical growth: the solute concentration on the solid side (dots) and liquid side (triangles) of the interface vs time. The solid line represents the interface velocity. The Lewis number is Le$=6.45\times10^{-9}$.

the maximum of T_I is 1701.9 K when $v=1225$; then the interface is suddenly decelerated, and a new transition again turns the process into a low velocity regime. This second transition was already identified by the author [20] in a previous study on planar solidification, and was explained through an analysis based on the comparison of the time scales for thermal and chemical diffusion. It was argued that, since $D_c/v^2 \ll D_T/v^2$, the phase and solute fields evolve with a (quasisteady) dynamics slaved by the local interface thermal conditions. As the $T_I(v)$ curve resulting from Eqs. (10) and (11) is a nonmonotonic function, both low and high velocity states are accessible to the growth process, and the sharp interface deceleration corresponds to the transition of the operating point from the high velocity branch to the low velocity branch. It is worth noting that sharp transitions between the high and low velocity branches of the $T_I(v)$ curve were also observed in the dynamics of the banding phenomena [18,27,28], and were ascribed to the same mechanism. The complex behavior of the process dynamics reflects on the solute segregation at the moving front. Figure 4 shows, c_s and c_l versus time, i.e. the solute concentration on the solid side (dots) and liquid side (triangles) of the interface. For clarity, on the same graph we superimposed a curve representing the interface velocity (solid line). The large concentration gap which characterizes the first stage of the process is suddenly closed at the first transition when, due to the high growth rate, the solute segregation is suppressed. Then the interface velocity decreases and solute partition again becomes effective; this corresponds to an increase of the solute concentration in the liquid. At a second sharp transition (toward the low velocity regime) we observe that the concentration gap is suddenly restored. The sharp transients which characterize the growth process leave a trace in the solidified alloy. In Fig. 5 we see the solute profile at t

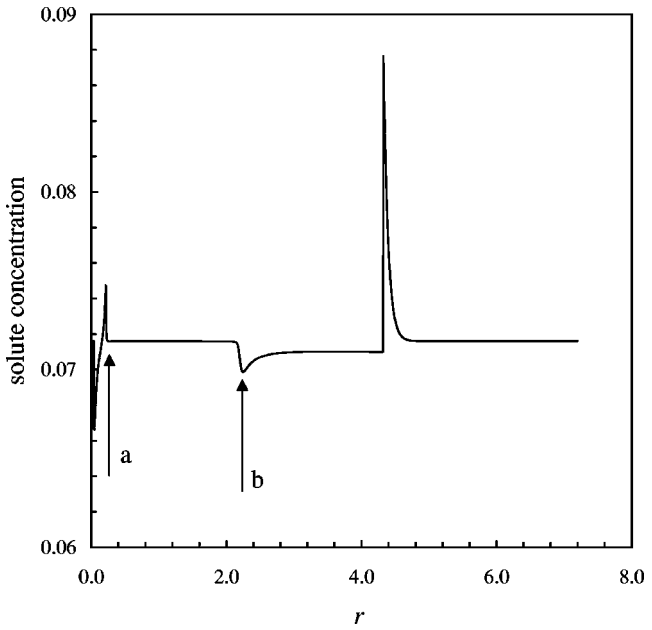

FIG. 5. Cylindrical growth: the concentration profile with Le $=6.45\times10^{-9}$, at time $t=10^{-1}$. The arrows (a) and (b) indicate the effects of the sharp variations of the growth rate.

$=10^{-1}$: we observe a positive peak (a) at $R^*=0.25$, which keeps the memory of the sudden incorporation into the solid of the solute excess at the first transition; the subsequent negative peak (b) reflects the depletion of solute on the solid side of the interface at the second transition.

The above results show the rich variety of dynamic regimes accessible to the solidification process in some regions of the parameters space. However, a simpler behavior arises for more realistic values of the thermal diffusivity. In Fig. 6 we show the data obtained with a larger value of the Lewis number, Le$=6.45\times10^{-5}$, typical of metallic alloys. In this case the rejection of heat becomes less effective and the interface warms up. According to Eqs. (10) and (11) the kinetic regime is prevented for $T_I>1702$ K. We observe that the interface temperature evolves well beyond this value; then the process enters a diffusive regime governed by the rejection of solute, and the growth rate approaches the power law $\propto t^{-1/2}$. These data show that for rapid alloy solidification the finite rate of heat rejection cannot be neglected, as it is precisely this effect which determines the main qualitative characteristics of the growth. The relaxation of the process towards equilibrium is also displayed through the inset in Fig. 6, where we see that the concentration gap at the interface c_l-c_s increases with time, approaching asymptotically the equilibrium value.

B. Spherical growth

In this case curvature effects are still persistent at a later stage of the crystal growth, as the curvature of a sphere is twice the one of a cylinder of the same radius. To prevent remelting we had to fix the initial radius of the germ as $R_0=0.08$. Figure 7 shows the interface velocity (solid line) and temperature (solid dots) versus time, for Le$=6.45\times10^{-9}$.

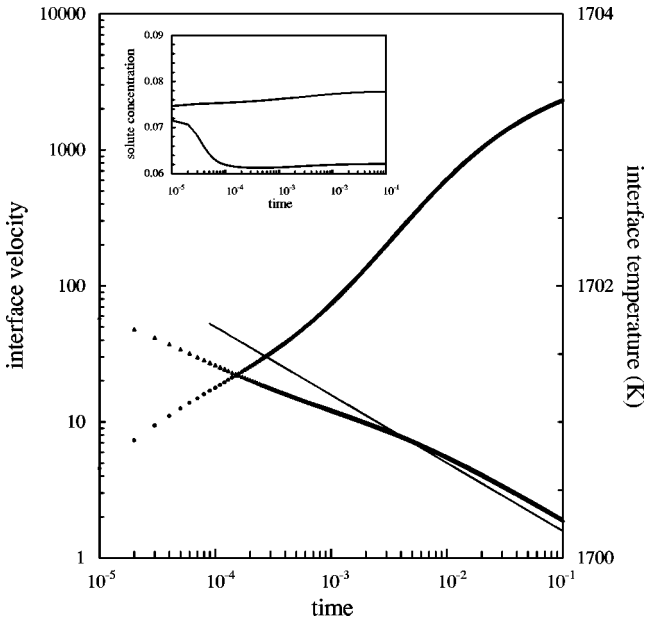

FIG. 6. Cylindrical growth: the interface velocity (triangles) and temperature (dots) vs time. Le$=6.45\times10^{-5}$. The straight line is representative of the power law $\propto t^{-1/2}$. The inset shows the solute concentration on the solid (lower curve) and liquid side (upper curve) of the interface.

This graph should be compared with the curves in Fig. 3. The transition to the thermal regime is retarded, and occurs at $t^*\sim5\times10^{-3}$ ($t^*\sim1.25\times10^{-3}$ in two dimensions). We should note that the radius of the crystal at the transition is $R^*=0.5$, that is exactly twice the value $R^*=0.25$ found for cylindrical growth. The further evolution of the process exhibits the same qualitative features observed in two dimensions: the interface is slowed down until, with a strong de-

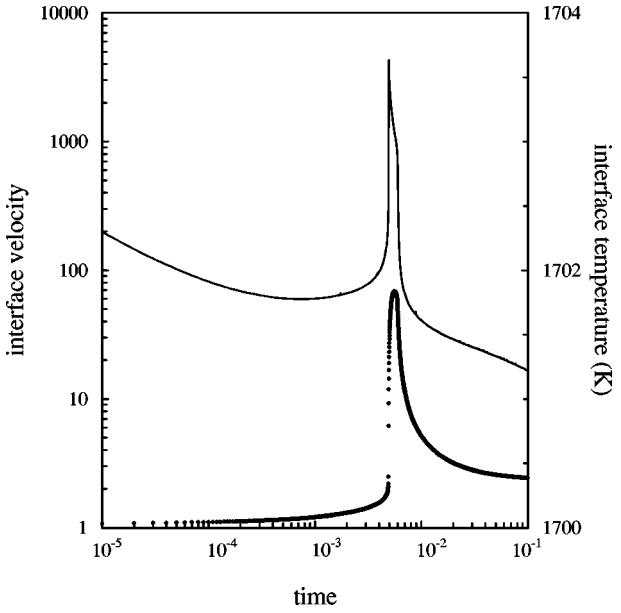

FIG. 7. Spherical growth: the interface velocity (solid line) and temperature (solid dots) vs time. The Lewis number is Le$=6.45\times10^{-9}$.

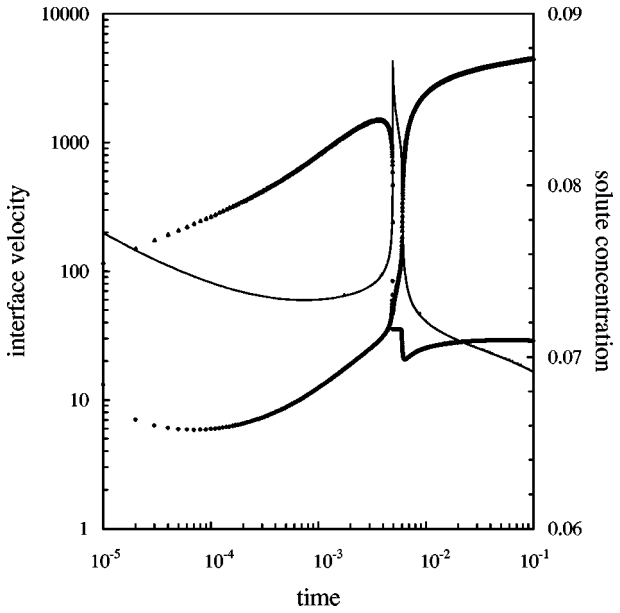

FIG. 8. Spherical growth: the solute concentration on the solid side (dots) and liquid side (triangles) of the interface vs time. The solid line represents the interface velocity. The Lewis number is $\mathrm{Le}=6.45\times10^{-9}$.

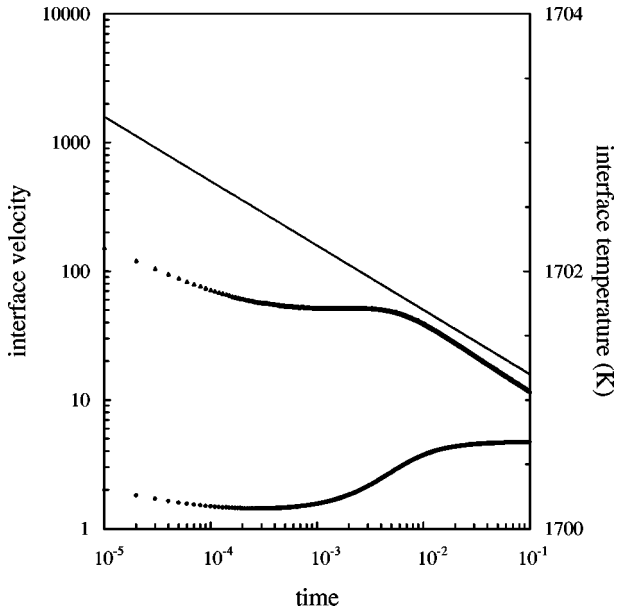

FIG. 9. Spherical growth: the interface velocity (triangles) and temperature (dots) vs time. $\mathrm{Le}=6.45\times10^{-5}$. The straight line is representative of the power law $\propto t^{-1/2}$.

celeration, the low velocity branch is reached. Figure 8 shows the time dependence of c_s and c_l; the interface velocity is also represented on the graph. Here too the solute concentration at the interface reflects the complex dynamics of the growth rate. We see the sudden suppression of the solute segregation subsequent to the transition to the thermal regime; the concentration gap is then restored when the low velocity branch is reached. It should be mentioned that the solute profile in the solidified alloy shows the same characteristics we observed in the two dimensional case.

Figure 9 shows the data obtained with $\mathrm{Le}=6.45\times10^{-5}$. As can be observed, the growth rate asymptotically approaches the $v\propto t^{-1/2}$ power law, while T_I saturates to a value slightly below 1701 K. We checked that in the R,v plane the trajectory described by the process lies all the time below the curve extracted from Eqs. (10) and (11), never intersecting it; this means that in this case a transition to the thermal regime is not allowed, and the growth rate is controlled by chemical diffusion.

V. CONCLUSIONS

The cylindrical or spherical solidification of binary alloys is generally addressed in the isothermal limit, and resorting to the quasistatic approximation. At large supersaturation this approach is not adequate, and the problem must be treated in its full time-dependent characteristics, accounting for both heat and solute diffusion. From this perspective, the interface dynamics reveals a rich variety of growth regimes. At low values of the Lewis number, in the late stage the growth is controlled either by the interface kinetics (in the limit $\mathrm{Le}=0$) or by thermal diffusion (for $\mathrm{Le}\neq0$). However, this behavior is not accessible to experimental observation, as it assumes too fast a heat rejection. At realistic values of the Lewis number the interface warms up, and the process enters a regime in which the rate limiting mechanism is the diffusion of solute. It is interesting to note that, even for metallic alloys (in which heat transport is much faster than solute transport), neglecting the finite rate of thermal diffusion dramatically changes the picture of the solidification process.

[1] J.S. Langer, Rev. Mod. Phys. **52**, 1 (1980).
[2] M.J. Aziz, J. Appl. Phys. **53**, 1158 (1982).
[3] M.J. Aziz and T. Kaplan, Acta Metall. **36**, 2335 (1988).
[4] M.J. Aziz and W.J. Boettinger, Acta Metall. **42**, 527 (1994).
[5] G. Caginalp and W. Xie, Phys. Rev. E **48**, 1897 (1993).
[6] G. Caginalp and J. Jones, Ann. Phys. (N.Y.) **237**, 66 (1995).
[7] A.A. Wheeler, W.J. Boettinger, and G.B. McFadden, Phys. Rev. A **45**, 7424 (1992).
[8] A.A. Wheeler, W.J. Boettinger, and G.B. McFadden, Phys. Rev. E **47**, 1893 (1993).
[9] M. Conti, Phys. Rev. E **55**, 701 (1997).
[10] M. Conti, Phys. Rev. E **56**, 3717 (1997).
[11] N.A. Ahmad, A.A. Wheeler, W.J. Boettinger, and G.B. McFadden, Phys. Rev. E **58**, 3436 (1998).
[12] Zhiqiang Bi and Robert F. Sekerka, Physica A **261**, 95 (1998).
[13] D.A. Kessler, J. Koplik, and H. Levine, Adv. Phys. **37**, 225 (1988).
[14] W. Kurz and D. J. Fisher, *Fundamentals of Solidification* (Trans Tech, Aedermannsdorf, 1992).
[15] S. R. Coriell and G. B. McFadden, in *Handbook of Crystal Growth*, edited by D.T.J. Hurle (Elsevier, Amsterdam, 1993).
[16] B. Caroli, C. Caroli, and B. Roulet, in *Solids Far from Equi-*

librium, edited by C. Godreche (Cambridge University Press, Cambridge, 1992).
[17] W.W. Mullins and R.F. Sekerka, J. Appl. Phys. **35**, 444 (1964).
[18] A. Karma and A. Sarkissian, Phys. Rev. Lett. **68**, 2616 (1992).
[19] A. Karma and A. Sarkissian, Phys. Rev. E **47**, 513 (1993).
[20] M. Conti, Phys. Rev. E **61**, 642 (2000).
[21] J.A. Warren and W.J. Boettinger, Acta Metall. Mater. **43**, 689 (1995).
[22] M. Conti, Phys. Rev. E **58**, 6166 (1998).
[23] S.L. Wang, R.F. Sekerka, A.A. Wheeler, B.T. Murray, S.R. Coriell, R.J. Braun, and G.B. McFadden, Physica D **69**, 189 (1993).
[24] R. Willnecker, D.M. Herlach, and B. Feuerbacher, Phys. Rev. Lett. **62**, 2707 (1989).
[25] M. Conti, Phys. Rev. E **55**, 765 (1997).
[26] M. C. Flemings, *Solidification Processing* (McGraw-Hill, New York, 1974).
[27] M. Carrard, M. Gremaud, M. Zimmermann, and W. Kurz, Acta Metall. Mater. **40**, 983 (1992).
[28] M. Conti, J. Cryst. Growth **198/199**, 1251 (1999).